J Petrol Explor Prod Technol (2017) 7:1165–1172
DOI 10.1007/s13202-017-0321-7

ORIGINAL PAPER - PRODUCTION ENGINEERING

Displacement efficiency in the water flooding process in fracture–vuggy reservoirs

Yi-Long Li[1] · Feng Wu[1] · Xiao-Ping Li[1] · Xiao-Hua Tan[1] · Xiao-Hua Hu[2] · Qiang Yang[1]

Received: 27 March 2016 / Accepted: 5 January 2017 / Published online: 28 January 2017
© The Author(s) 2017. This article is published with open access at Springerlink.com

Abstract To determine how fracture–vuggy structure, pressure, and injection–production mode influence displacement efficiency in the water flooding process in fracture–vuggy reservoirs, two types of models were built based on the characteristic of such reservoir: two fracture models with different fracture apertures and two fracture–vuggy models with different sizes of vugs. A series of two-phase fluid flow experiments was conducted to study oil and water distribution as well as flow pattern in the water flooding process. Results show that displacement efficiency is significantly influenced by injection–production mode and injection pressure. By contrast, its relationship with the size of vugs is insignificant. Under the same injection–production mode, high-to-low recovery that corresponds to model type includes the small fracture, large fracture, small vug, and large vug models. Under the same pore volume multiple, high-to-low recovery that corresponds to model includes the small fracture, small vug, large fracture, and large vug models.

Keywords Fracture–vuggy · Water flooding · Flow pattern · Injection–production mode · Displacement efficiency

✉ Xiao-Ping Li
lixiaoping@swpu.edu.cn

✉ Xiao-Hua Tan
xiaohua-tan@163.com

[1] State Key Laboratory of Oil-Gas Reservoir Geology and Exploitation, Southwest Petroleum University, Chengdu, China

[2] Exploration and Development Research Institute, Southwest Oil and Gas Field Branch, Chengdu, China

Introduction

The Tahe (TH) fracture–vuggy reservoirs in Xinjiang, China, are buried at considerable depths, exhibit strong heterogeneity, and are difficult to develop (Popov et al. 2009; Gu and Chalaturnyk 2010; Noushabadi et al. 2011). Fractures provide the oil-storing spaces and flow channels of a reservoir. Vugs are one of the most important oil-storing spaces in a reservoir (Chen et al. 2005; Corbett et al. 2010). Waterflood has been used to develop reservoirs and the recovery efficiency has increased approximately 10% (Tu 2008). However, the result is not as good as expected. The flow pattern in fracture–vuggy system, which is the elementary cell of this type of reservoir, must be determined to improve recovery (Zhang et al. 2016).

Numerous studies have been conducted on this subject. Analytical expressions to characterize a spontaneous cocurrent imbibition process of the wetting fluid into gas-saturated porous media were proposed based on the fractal characteristics of porous media (Cai et al. 2010a, b). Cai et al. (2010a, b) presented a fractal capillary model to analyze the depth of extraneous fluid invasion and concluded that the tortuosity of the capillaries and capillary pressure should be considered in analyzing extraneous fluid invasion in low-porosity porous media. Cai et al. (2012) presented a complete analytical model to characterize the vertical spontaneous imbibition of wetting liquid into gas-saturated porous media based on the fractal characteristics of pores in porous media; they also analyzed the influencing factors of the imbibition process. Cai et al. (2014) presented a generalized model that could describe the time evolution of spontaneous imbibition for many wetting liquids in natural and artificial porous media based on the modified H − P and L − Y equations. Tan et al. (2015c, d) presented a model for transient flow in porous media based

on the fractal properties of tree-shaped capillaries and generalized Darcy's law. They believed that the fractal characteristics of the tree-shaped fractal networks should be considered in analyzing transient flow in heterogeneous porous media. Zhang et al. (2015) presented a new semi-analytical model for vertical wells with simulated reservoir volume (SRV). A model that could approximately reproduce the global trend of the variation in the time exponent with changing porosity was derived for capillary imbibition in porous media based on the tortuous capillary model and fractal geometry (Cai and Yu 2011). Tan et al. (2015c, d) presented a permeability model for porous media that considered the stress sensitivity based on the mechanics of materials and the fractal characteristics of solid cluster size distribution. Su et al. (2015) presented an improved second-order finite element mixed model for fluid flow in constricted reservoirs. Sensitivity analyses were performed to determine the effects of the threshold pressure gradient and the permeability of various media. The result shows that increasing the permeability of artificial fractures is a suitable strategy to raise the actual bottom hole pressure, but only in low-permeability matrices. Tan et al. (2015a, b) presented novel predictive models for the permeability and porosity of porous media. These models, which considered stress sensitivity, were based on fractal theory and the mechanics of materials.

To study the flow pattern more intuitively, numerous physical models have been built and related experiments have been performed. Two types of models were constructed to obtain the relative permeability curves; the results showed that fracture aperture, fracture network structure, vug density, and vug porosity had different effects on relative permeability, and that the influence effect exhibited evident regularity (Lv et al. 2011). Zeng et al. (2011) considered that the single-phase oil–water flow in ultra-low-permeability cores was inconsistent with Darcy's law. A typical flow curve is a combination of a straight line and a concave curve. When the permeability of the core is low, the nonlinearity of the concave curve is strong. Lian and Cheng (2012) conducted experiments on the oil–water relative permeability of carbonate cores from the Kenkiyak oil field and compared the differences in relative permeability curves between the natural matrix cores and the artificial fracture cores. Their study showed that water injection should be implemented when reservoir pressure was relatively higher to maintain formation pressure during water flooding and reduce the effect of stress sensitivity. Dong et al. (2013) studied the influencing factors of the relative permeability of oil and water in a single fracture. The result showed that relative permeability decreases with increasing water–oil viscosity ratio, decreasing fracture aperture, and increasing displacement velocity. Karimaie and Torsæter (2007) assumed that the oil production rate increased with increasing initial water saturation, and breakthrough oil recovery was higher when the water injection rate was low. Hou et al. (2014) performed a macroscopic 3D physical study of the water breakthrough pattern of fracture–vuggy reservoirs. The result showed the water breakthrough time was controlled by the connectivity of the well to the bottom water. Tong et al. (2015) believed that intermittent injection could optimize the function of oil–water gravity segregation, thereby reducing water cut and significantly improving the production rate of the initial stages compared with continuous injection. The distribution law of the remaining oil in the fracture-cavity reservoir was studied based on full diameter cores (Wang et al. 2012, 2014). The result showed the remaining oil after primary water flooding, which includes "attic oil," "occlusion oil," "oil film," "corner oil," and "blind cavity oil." These researchers believed that the remaining oil could be recovered via secondary water flooding, gas injection, chemical flooding, fracturing, and other stimulation measures.

The TH fracture–vuggy reservoir is different from other types of reservoir. The porosity and permeability of its matrix can be disregarded. The 3D data cubes of the reservoir show that the diameter of the main cavities is 8–100 m, whereas the diameter of the fractures is 0.001–0.03 m. Fluid flow in this type of reservoir can be regarded as pipe flow. All studies in microscale are based on seepage theory. Several scholars (Wang et al. 2014) studied the remaining oil distribution law based on macro-physical models; however, these models are invisible. In practical production, factors, such as the relative positions of the injection–production wells and reservoirs, water injection pressure, and injection pore volume multiple (PV), significantly affect reservoir recovery in water injection process. So it is necessary from these macro-aspects to study the flow pattern in a fracture–vuggy system from macro-aspects and is necessary to provide experimental and theoretical bases for selecting the injection–production mode and water flooding adjustment.

Experimental model and fluid properties

Introduction to the model

The wettability of the core of the TH oil field is slightly oil–wet. Thus, an organic glass plate (with high transparency and strength, light quality, and easy processing), with a wettability similar to that of the core, is used to build physical models. The transparency of the organic glass plate is utilized to record the distribution of oil and water that flow together in the fracture–vuggy by taking photographs. Then, the regular oil and water distribution in the

water injection process can be summarized by analyzing the photographs.

Four basic models are built: MX1, MX2, MX3, and MX4. MX1 and MX3 are both fracture models with different fracture apertures at the center of the models. MX2, which has two matching small vugs, and MX4, which has a large vug, are both fracture–vuggy models. To simulate the relative position of the wells and the reservoir, three small channels are set on both sides of the models. These channels are known as high-, middle-, and low-position channels. The schematic diagrams of the models are shown in Fig. 1a–d. The parameters of the models are shown in Table 1.

Properties of the experimental fluid

Experimental oil and mixed water, which are combined with distilled water and edible salt to simulate formation water, are selected as experimental fluids. Mixed water is stained black using ink to distinguish between experimental oil and mixed water.

At 25 °C, the density and viscosity of mixed water are 1.0099 g/cm^3 and 2.7349 mpa.s, respectively. The experimental oil is 36# auxiliary oil, whose density and viscosity are 0.8507 g/cm^3 and 9.0235 mpa.s at 25 °C, respectively.

Experimental procedure

The experimental flowchart is shown in Fig. 2. The procedure of experiment is described as follows:

(1) The model is saturated with experimental oil. Oil is injected into the system from the left side of the system. During this procedure, air bubbles are pushed out by the oil injection. The entire flow system must be guaranteed to be full of oil before proceeding to the following steps.
(2) The low-position channel on the left side of the model is connected to the injection pipeline, and the high-position channel on the right side of the model is connected to the output line.
(3) The valve that is directly connected to the water tank is opened. The mixed water is injected into the model following a preset pressure. Water–oil mixture from the model is separated using an oil–water separator, and the data are recorded. The valve is closed when the water cut reaches 98%. In the experiment process, the oil–water distribution is recorded using a video system.
(4) The pressure of the injection water is changed. Steps (2) and (4) are iterated.
(5) The positions of the injection and output channels are changed. The high-position channel on the left side of the model is connected to the injection pipeline, and the low-position channel on the right side of the model is connected to the output line. Steps (2), (4), and (5) are iterated.
(6) The positions of the injection and output channels are changed. The high-position channel on the left side of the model is connected to the injection pipeline, and the high-position channel on the right side of the model is connected to the output line. Steps (2), (4), and (5) are iterated.

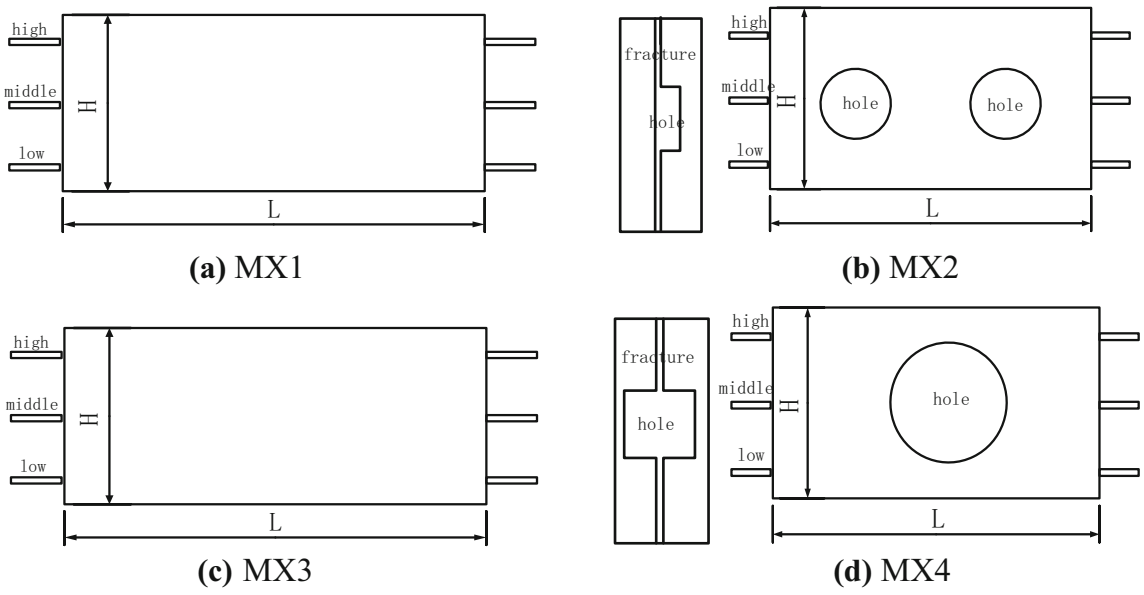

Fig. 1 Chart of basic models

Table 1 Parameters of the basic models

Model numbers	Length (mm)	Height (mm)	Fracture aperture (mm)	Dip angle (°)	Volume (ml^3)	Vug thickness (mm)	Vug diameter (mm)
MX1	208.5	92.3	1	80	13.80		
MX2	209.0	93.0	1	80	28.15	5.0	17.60
MX3	209.0	93.0	2	80	27.60		
MX4	208.0	92.0	1	80	63.12	37.9	49.23

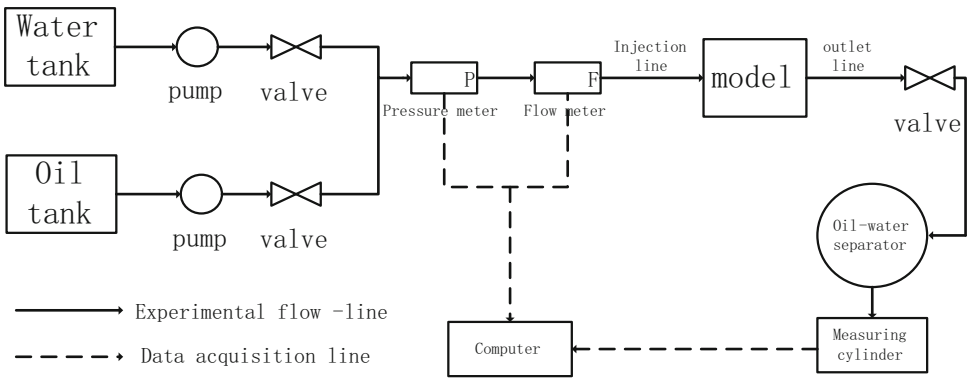

Fig. 2 Chart of experimental flow

(7) Data and images are sorted. The oil–water distribution is analyzed, and the flow pattern in the water injection process is concluded.

Experimental results and analysis

Oil and water distribution rule

Basic fracture models

In this experiment, MX1 and MX3 are selected as the experimental models, and their fracture apertures are 1 and 2 mm, respectively. The flowing differential pressure is approximately 500 Pa. The temperature of the experiment is 25 °C.The fracture dip is 80°.

MX1 and MX3 are both basic fracture models with different fracture apertures. Figures 3 and 4 show the oil and water distribution at different times when water flows in from the low-position channel and flows out from the high-position channel in MX1 and MX3, respectively. These figures can be analyzed as follows. As the time of injection increases, water can spread to a larger area with a smaller fracture aperture. Capillary force is more significant, and the effect of gravity is weaker with a smaller crack.

Figure 5 shows the oil and water distribution at different times when water flows in from the high-position channel and flows out from low-position channel in MX3. Figure 5 can be analyzed as follows. When water flows in MX3, water, which has higher density, occupies the upper portion of the model, whereas oil, which has lower density, stays in the lower part of the model. As injection time increases, water gradually spreads to the lower part of the model under the action of gravity. However, the difference of oil–water density (0.8507/1.0099) is small; thus, water flows out of the model and fails to replace oil completely.

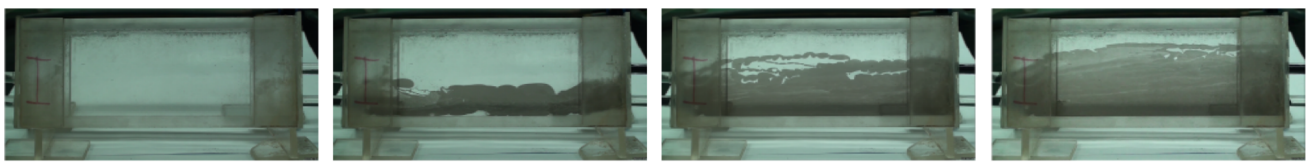

Fig. 3 Chart of oil and water distribution at different times when water flows in from the low-position channel and flows out from the high-position channel in MX1

Fig. 4 Chart of oil and water distribution at different times when water flows in from low-position channel and flows out from the high-position channel in MX3

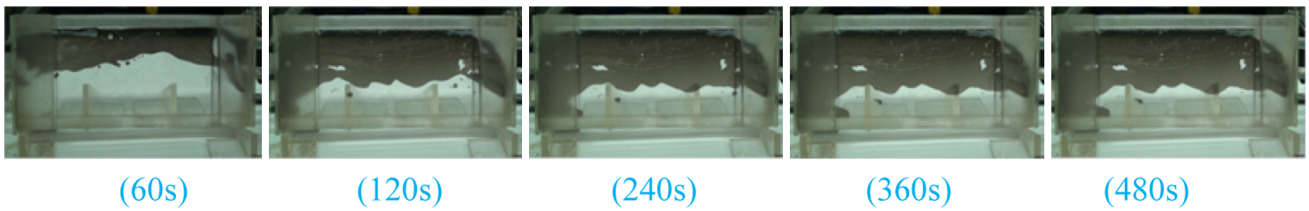

Fig. 5 Chart of oil and water distribution at different times when water flows in from the high-position channel and flows out from the low-position channel in MX3

Basic fracture–vuggy models

In this experiment, MX2 and MX4 are selected as experimental models. Their fracture apertures are the same, but the sizes of their vugs differ. Flowing differential pressure is approximately 500 Pa. The temperature of experiment is 25 °C. The fracture dip is 80°.

The photographs of oil and water distribution at different times in MX2 and MX4 are shown in Figs. 6, 7, 8 and 9. Figures 6 and 8 show water flows from the bottom of the models and begins to enter the caves after oil–water interface reaches the bottom of the caves under low–high mode. However, water will enter the caves from the middle–upper part of the caves under high–low mode as shown in Figs. 7 and 8. In MX2, when water flows into the vug, the role of gravity is dominant and the oil–water interface is evident. However, a certain amount of time is still required for oil and water to separate. In MX4, oil–water separation is performed simultaneously with water injection, and the interface is generally horizontally uplifted in vugs.

Oil and water flow pattern

Influence of injection pressure on recovery percent

In this section, experiments are conducted under low pressure (500 Pa) and high pressure (800 Pa). For MX1 and MX4, water flows in from the low-position channel and flows out from the high-position channel. For MX2 and MX3, water flows in from the high-position channel and flows out from the low-position channel.

The curves of the recovery percent with different injection pressures in MX1 and MX4 are shown in Fig. 10. The curves of the recovery percent with different injection pressure in MX2 and MX3 are shown in Fig. 11. Figure 10 shows that better displacement efficiency can be achieved with higher injection pressure with the same PV; however, this result is contrary to that shown in Fig. 11.

In MX1 and MX4, which have low-position injection and high-position production, the flow rate of oil–water increases with the increase in injection pressure. Then, the oil gathering on the edge of the models is more easily

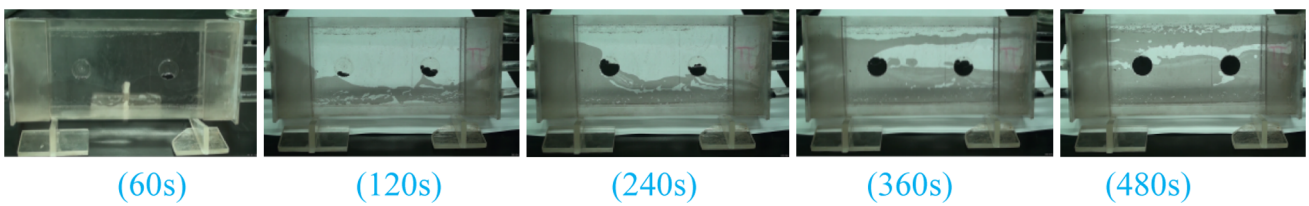

Fig. 6 Chart of oil and water distribution at different times when water flows in from the low-position channel and flows out from the high-position channel in MX2

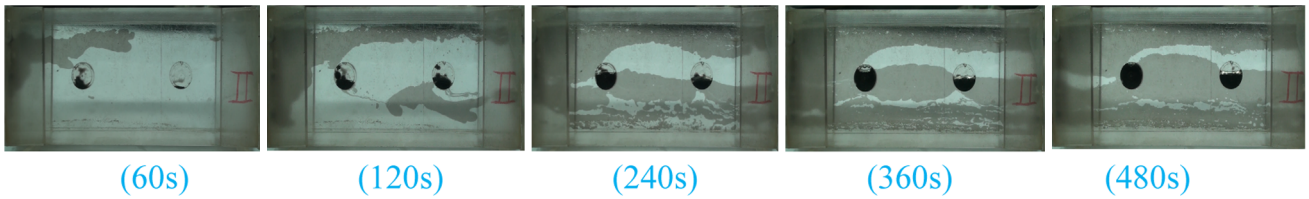

Fig. 7 Chart of oil and water distribution at different times when water flows in from the high-position channel and flows out from the low-position channel in MX2

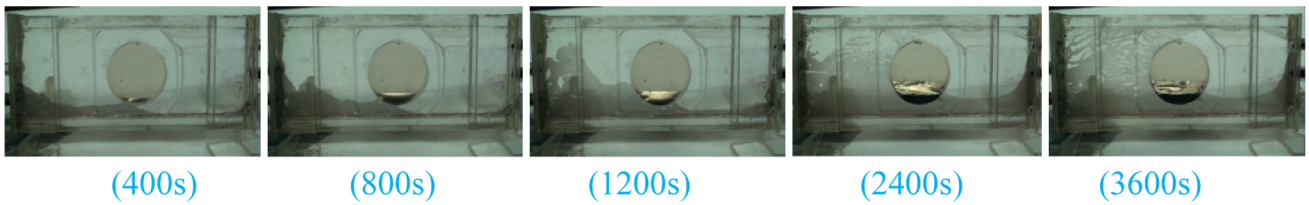

Fig. 8 Chart of oil and water distribution at different times when water flows in from the low-position channel and flows out from the high-position channel in MX4

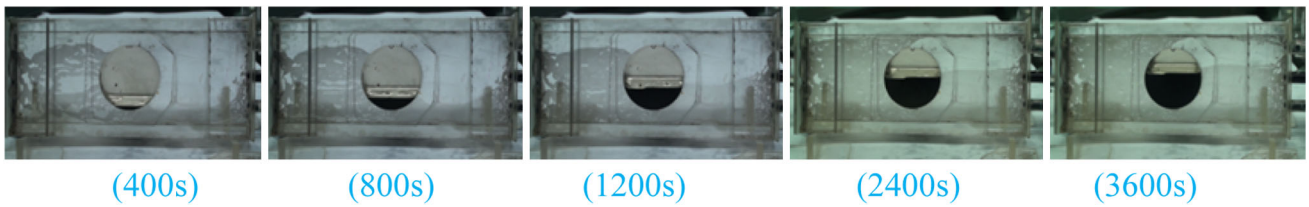

Fig. 9 Chart of oil and water distribution at different times when water flows in from the high-position channel and flows out from the low-position channel in MX4

Fig. 10 Chart of recovery percent with different injection pressures in MX1 and MX4

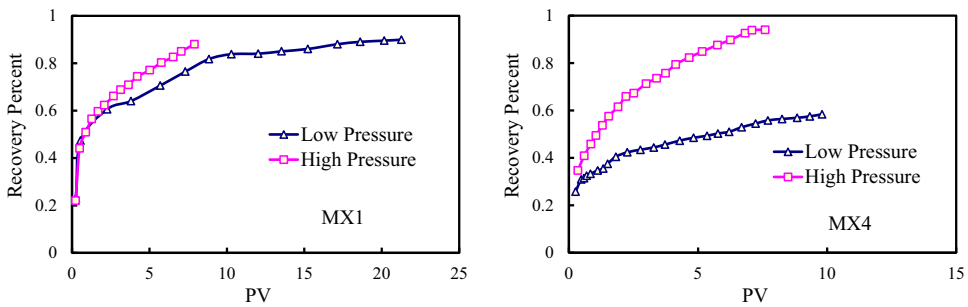

Fig. 11 Chart of recovery percent with different injection pressures in MX2 and MX3

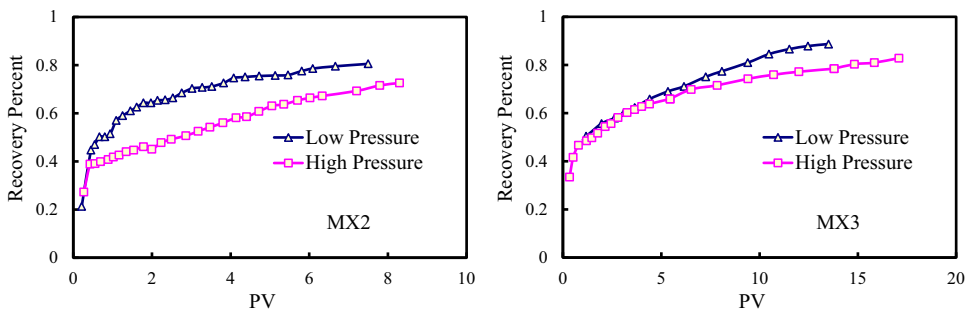

displaced. Thus, displacement efficiency increases. In MX2 and MX3, which have high-position injection and low-position production, the flow rate of oil–water increases with the increase in injection pressure. Then the effect of gravity decreases. Water flows out of the model and has no time to fully replace oil.

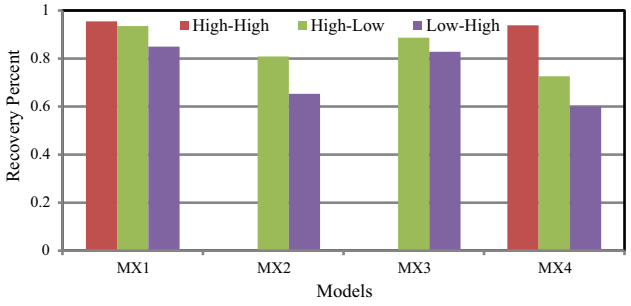

Fig. 12 Chart of recovery percent with varying injection–production positions in different models

Influence of injection–production position on recovery percent

The recovery percent with varying injection–production positions in different models are shown in Fig. 12. This figure can be analyzed as follows.

(1) For the same type of model, the high-to-low recovery that corresponds to the injection–production position is as follows: high-position injection and high-position production, high-position injection and low-position production, and low-position injection and high-position production.
(2) For the same injection–production position, the high-to-low recovery that corresponds to model type is as follows: the small fracture, large fracture, small vug, and large vug models.

Influence of PV on recovery percent

Under the low-position injection and high-position production mode, the recovery percent with PV in different models are shown in Fig. 13. This figure can be analyzed as follows.

(1) The recovery percent increases and the degree of increase gradually slows down with the increase in PV.

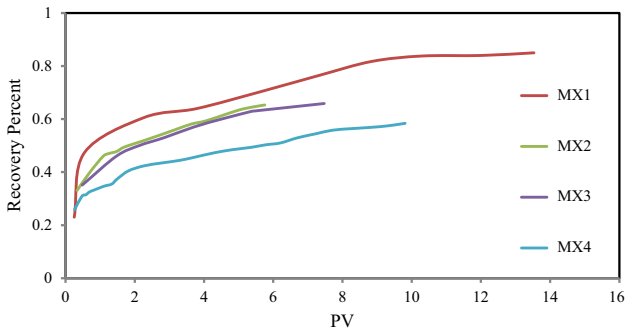

Fig. 13 Chart of recovery percent with PV

(2) Under the same PV, the high-to-low recovery that corresponds to the model type is as follows: the small fracture, small vug, large fracture, and large vug models.

Conclusion

In this work, the distribution and flow pattern of water and oil in the water flooding process are studied based on the basic fracture and fracture–vuggy models. The main conclusions can be summarized as follows.

(1) For the fracture models under low-position injection and high-position production mode, the displacement effect is more evident when fracture aperture is large. Water mainly exhibits a lateral displacement function in the high-position injection and low-position production mode, and vertical gravity differentiation is unapparent.
(2) For the fracture–vuggy models, the oil–water interface of the vugs is generally horizontally uplifted. The larger the vugs, the more evident the effect of gravity. Consequently, the gravitational differentiation effect will be better.
(3) When injection–production wells are located in the fracture–vuggy system, displacement efficiency is significantly influenced by injection–production position and injection pressure; it also has minimal relation to the size of vugs. In the high-position injection and low-position production mode, displacement efficiency decreases with the increase in injection pressure. In the low-position injection and high-position production, displacement efficiency increases with the increase in injection pressure.
(4) For the same type of model, the high-to-low recovery corresponds to the injection–production position is as follows: high-position injection and high-position production, high-position injection and low-position production, and low-position injection and high-position production.
(5) Under the same injection–production position, the high-to-low recovery corresponds to model type is as follows: the small fracture, large fracture, small vug, and large vug models.
(6) Under the same PV, the high-to-low recovery corresponds to model type is as follows: the small fracture, small vug, large fracture, and large vug models.

Acknowledgements The authors would like to thank the reviewers for positive and invaluable suggestions, which have greatly improved the manuscript. This work was partly supported by the National Natural Science Foundation of China under Grant No. 51374181 and the Research Fund for the Doctoral Program of Higher Education of China under Grant No. 20115121120002.

Open Access This article is distributed under the terms of the Creative Commons Attribution 4.0 International License (http://creativecommons.org/licenses/by/4.0/), which permits unrestricted use, distribution, and reproduction in any medium, provided you give appropriate credit to the original author(s) and the source, provide a link to the Creative Commons license, and indicate if changes were made.

References

Cai J, Yu B (2011) A discussion of the effect of tortuosity on the capillary imbibition in porous media. Transp Porous Med 89:251–263

Cai J, Yu B, Zou M, Luo L (2010a) Fractal characterization of spontaneous co-current imbibition in porous media. Energy Fuels 24:1860–1867

Cai J, Yu B, Zou M, Mei M (2010b) Fractal analysis of invasion depth of extraneous fluids in porous media. Chem Eng Sci 65:5178–5186

Cai J, Hu X, Standnes DC, You L (2012) An analytical model for spontaneous imbibition in fractal porous media including gravity. Colloids Surf A 414:228–233

Cai J, Edmund P, Cheng C, Hu X (2014) Generalized modeling of spontaneous imbibition based on hagen-poiseuille flow in tortuous capillaries with variably shaped apertures. Langmuir 30:5142–5151

Chen ZH, Yong D, Lang ZX (2005) Storage percolation modes and production performance of the karst reseroirs in Tahe Oilfield. Pet Explor Dev 32:101–105

Corbett PWM, Geiger-Boschung S, Borges LP, Garayev M, Gonzalez JG, Valdez C (2010) Limitations in numerical well test modelling of fractured carbonate rocks. In: SPE EUROPEC/EAGE annual conference and exhibition, Society of Petroleum Engineers

Dong Z, Aifen L, Qiang S, Yanqing F (2013) Measuring oil and water relative permeability in a single fracture and researching its impacting factors. Pet Sci Technol 31:2191–2201

Gu F, Chalaturnyk R (2010) Permeability and porosity models considering anisotropy and discontinuity of coalbeds and application in coupled simulation. J Petrol Sci Eng 74:113–131

Hou J, Haibo LI, Jiang Y, Luo M, Zheng Z, Zhang L, Yuan DY (2014) Macroscopic three-dimensional physical simulation of water flooding in multi-well fracture-cavity unit. Pet Explor Dev 41:784–789

Karimaie H, Torsæter O (2007) Effect of injection rate, initial water saturation and gravity on water injection in slightly water-wet fractured porous media. J Petrol Sci Eng 58:293–308

Lian P, Cheng L (2012) The characteristics of relative permeability curves in naturally fractured carbonate reservoirs. J Can Pet Technol 51:137–142

Lv A, Yao J, Wang W (2011) Characteristics of oil–water relative permeability and influence mechanism in fractured-vuggy medium. Proc Eng 18:175–183

Noushabadi MRJ, Jourde H, Massonnat G (2011) Influence of the observation scale on permeability estimation at local and regional scales through well tests in a fractured and karstic aquifer (Lez aquifer, Southern France). J Hydrol 403:321–336

Popov P, Qin G, Bi L, Efendiev Y, Kang Z, Li J (2009) Multiphysics and multiscale methods for modeling fluid flow through naturally fractured carbonate Karst reservoirs. SPE Reserv Eval Eng 12:218–231

Su Y, Li B, Xu C, Hao Y (2015) Coupling fluid flow model of multiscale fractures in tight reservoirs. Proc Eng 126:353–357

Tan XH, Li XP, Liu JY, Zhang LH, Cai J (2015a) A model for transient flow in porous media embedded with randomly distributed tree-shaped fractal networks. Int J Modern Phys B 29(19):1550135

Tan XH, Li XP, Liu JY, Zhang LH, Cai J (2015b) Fractal analysis of stress sensitivity of permeability in porous media. Fractals Complex Geometry Patterns Scaling Nat Soc 23(2):1550001

Tan XH, Li XP, Liu JY, Zhang LH, Fan Z (2015c) Study of the effects of stress sensitivity on the permeability and porosity of fractal porous media. Phys Lett A 379:2458–2465

Tan XH, Liu JY, Li XP, Zhang LH, Cai J (2015d) A simulation method for permeability of porous media based on multiple fractal model. Int J Eng Sci 95:76–84

Tong KJ, Liu HQ, Zhang YC, Wang J, Ge LZ, Dai WH, Hong C, Meng QB (2015) Three-dimensional physical modeling of waterflooding in metamorphic fractured reservoirs. Pet Explor Dev 42:589–596

Tu XW (2008) Successful practice for carbonate reservoir development by cyclic water injection process. Xinjiang Pet Geol 29:735–736

Wang J, Liu H, Xu J, Zhang H (2012) Formation mechanism and distribution law of remaining oil in fracture-cavity reservoirs. Pet Explor Dev 39:624–629

Wang J, Liu H, Ning Z, Zhang H, Cheng H (2014) Experiments on water flooding in fractured-vuggy cells in fractured-vuggy reservoirs. Pet Explor Dev 41:74–81

Zeng B, Cheng L, Li C (2011) Low velocity non-linear flow in ultra-low permeability reservoir. J Petrol Sci Eng 80:1–6

Zhang Q, Su Y, Wang W, Sheng G (2015) A new semi-analytical model for simulating the effectively stimulated volume of fractured wells in tight reservoirs. J Nat Gas Sci Eng 27:1834–1845

Zhang N, Yao J, Xue SF, Huang ZQ (2016) Multiscale mixed finite element, discrete fracture–vug model for fluid flow in fractured vuggy porous media. Int J Heat Mass Transf 96:396–405